The Biophysicist

Visualization of Tethered Particle Motion with a Multidimensional Simulation

Khovesh Ramdin[1], Markus Hackl[2], Shishir P.S. Chundawat[2,*]

[1]Department of Physics and Astronomy, Rutgers, The State University of New Jersey, Piscataway, NJ, USA
[2]Department of Chemical and Biochemical Engineering, Rutgers, The State University of New Jersey, Piscataway, NJ, USA

ABSTRACT The analysis of particles bound to surfaces by tethers can facilitate understanding of biophysical phenomena (e.g., DNA–protein or protein–ligand interactions and DNA extensibility). Modeling such systems theoretically aids in understanding experimentally observed motions, and the limitations of such models can provide insight into modeling complex systems. The simulation of tethered particle motion (TPM) allows for analysis of complex behaviors exhibited by such systems; however, this type of experiment is rarely taught in undergraduate science classes. We have developed a MATLAB simulation package intended to be used in academic contexts to concisely model and graphically represent the behavior of different tether–particle systems. We show how analysis of the simulation results can be used in biophysical research using single-molecule force spectroscopy (SMFS). Students in physics, engineering, and chemistry will be able to make connections with principles embedded in the field of study and understand how those principles can be used to create meaningful conclusions in a multidisciplinary context. The simulation package can model any given tether–particle system and allows the user to generate a parameter space with static and dynamic model components. Our simulation was successfully able to recreate generally observed experimental trends by using acoustic force spectroscopy (AFS). Further, the simulation was validated through consideration of the conservation of energy of the tether–bead system, trend analyses, and comparison of particle positional data from actual TPM in silico experiments conducted to simulate data with a parameter space similar to the AFS experimental setup. Overall, our TPM simulator and graphical user interface is primarily for demonstrating behaviors characteristic to TPM in a classroom setting but can serve as a template for researchers to set up TPM simulations to mimic a specific SMFS experimental setup.

KEY WORDS foundational biophysics; single-molecule spectroscopy; computational methods and bioinformatics; force spectroscopy and scanning probe microscopy; computer-based teaching tools

I. INTRODUCTION

Visualizing, monitoring, and modeling the complex motion of a particle attached to an extensible tether in a viscous fluid environment (also referred to as tethered particle motion [TPM]) is relevant to understanding several fundamental biophysical phenomena, as well as solving practical engineering problems. Understanding and modeling TPM can enable experimentalists to observe the motion of DNA-scale molecular interactions by using immunofluorescence or dark-field microscopy (1) or to manipulate such small-scale systems with

"*" corresponding author

Received: 30 November 2022
Accepted: 6 October 2023
Published: 12 January 2024

molecular-scale precision by using suitable acoustic, magnetic, or optical tweezers as TPM imaging tools (2). Further, the advancements in the spatial resolution of optical imaging in the last few decades (3) have made TPM analysis particularly relevant to modern-day theoretical and applied biophysics. Particularly, understanding and modeling TPM is also critical for enabling single-molecule experiments that focus on various biopolymers and relevant molecular properties. For example, DNA polymer properties can be intrinsically studied and experimentally determined by using TPM modeling by analyzing the Brownian motion of particles attached to individual double-stranded DNA (4). Schafer et al. were one of the first to devise a TPM assay to directly monitor the movement of a single molecule of processive polymerases acting on a template DNA (4). Additional notable results that were achieved in subsequent studies include the empirical validation of TPM as a technique to predict tether length (5). Similar TPM and other single-molecule assays have become more commonplace now to provide critical insight into how diverse classes of biologic machinery and processive motors, e.g., cellulases and chitinases degrading cellulose and chitin polysaccharides (6–8); cellulose synthases synthesizing cellulose polymers (9); protein, DNA, and RNA polymer synthesis, folding, and degradation (10–12); and adenosine triphosphate–triggered motility of myosin and kinesin on actin and microtubules (13, 14), function at the molecular and cellular level to solve diverse biotechnology problems, ranging from developing better enzymes for producing sustainable bioenergy from cellulosic biomass (15) to enabling personalized health care using advanced gene-editing techniques such as CRISPR (16).

While described in the scientific literature, TPM is not typically taught in an academic context although the theory associated with this topic is crucial to understanding observations from many biophysical experiments. It is particularly necessary to study molecular-scale interactions by using single-molecule experiments incorporating TPM methods for comprehension of complex biomolecular and cellular systems that subsequently allow for improved fundamental understanding of living systems and potentially lead to the development of novel biotechnology.

II. SCIENTIFIC AND PEDAGOGIC BACKGROUND

Mathematically, tethered particle system behaviors can be approximated through the consideration of Brownian motion. Such motion is a consequence of collisions that occur between the object being tracked and the particles present in a viscous environment (17). In principle, fluids are composed of multiple particles that are constantly colliding. Such uncontrolled and seemingly random small-scale behaviors are better modeled stochastically, because deterministic models often require an unfeasible level of complexity for individual particle tracking capabilities (18). The idea associated with such models is to use random fluctuations to account for small-scale perturbations that are observed experimentally due to diffusive effects experienced by a particle in a viscous environment (19).

Here, we present a graphical user interface (GUI) simulation package for use by students and teachers to perform simulations of a model tether–particle system within a parameter space of choice (see illustration in Fig 1). The simulation was developed by using a complete installation of MATLAB (version 2022b; The MathWorks, Natick, MA).The simulation package builds and expands on previous models developed for educational purposes (20). The MATLAB-based model was written in an easily generalizable manner, has a complete user interface, and is computationally efficient, so data analyses can be easily performed. Simulation features such as varying force ramps and constant force application are predefined settings in the simulation package, because these are commonly encountered during single-molecule force spectroscopy (SMFS) experiments to mimic real-world scenarios (21). Further, corrections are included from a series of models presented in scientific literature to increase the

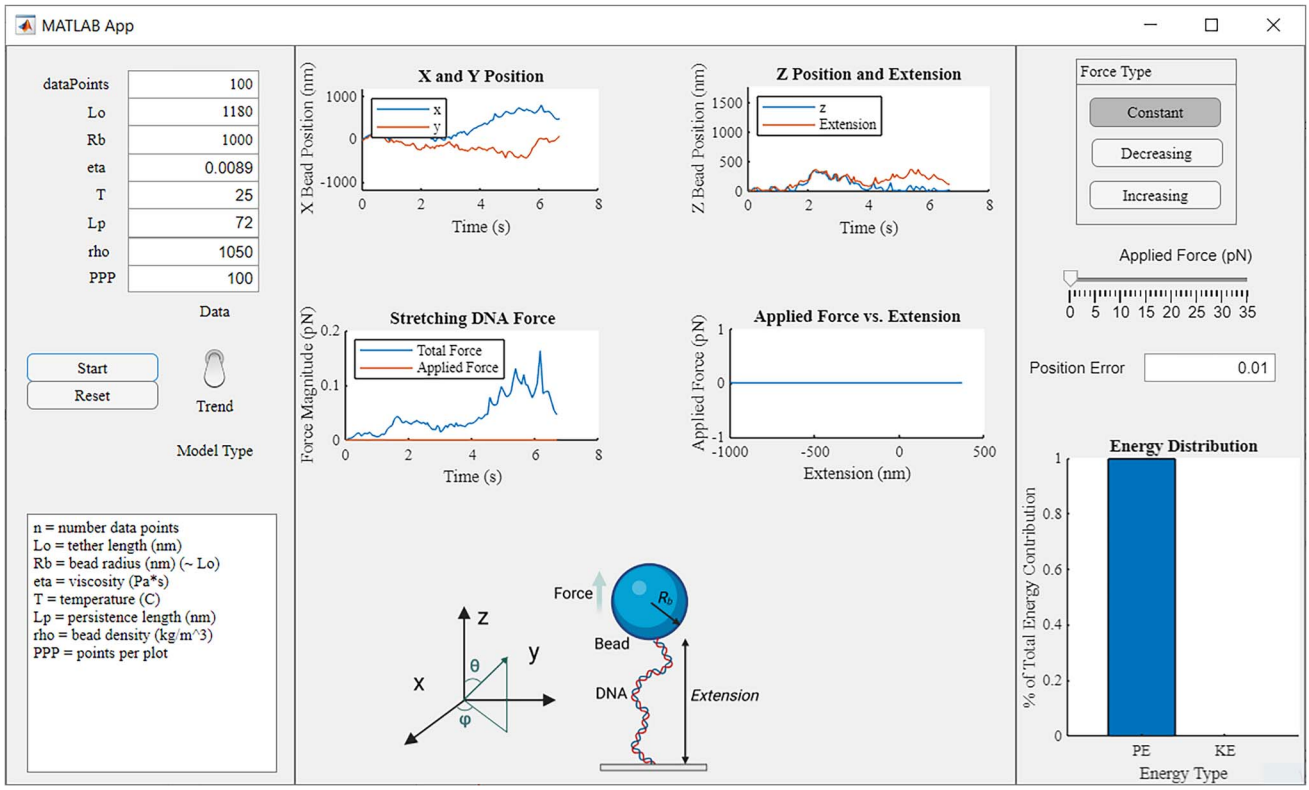

Fig 1. Overview of GUI for TPM simulation developed in this work. The left panel accepts inputs for simulation parameters and type of simulation model and has a simulation start and reset button, which updates and clear the plots. The middle panel includes the simulated data plots that are updated as the simulation runs. At the bottom of the middle panel, there is a sketch of the system being simulated. The right panel includes different options for force application that can be modified during the simulation run time or before it starts. There is also an energy validation plot at the bottom right corner of the GUI. The DNA bead sketch in Figure 1 was generated by using Biorender.com.

accuracy of the TPM simulations and allow the user to understand the limitations and uses of the calculations being made. In particular, we have generated experimental data to validate our simulation predictions using acoustic force spectroscopy (AFS) (22, 23). Students will be able to understand the behaviors of tethered particle systems in general due to the easy-to-follow GUI for model presentation and exportation of several analysis plots and data from the interface to gain an appreciation for how such systems dynamically behave during SMFS experiments.

A biophysics lab course would be ideal for presenting this information because the skills taught are relevant to both theoretic and experimental science. Single-molecule studies are associated with and based on concepts from optics, chemical bond theory, cellular machinery, and many other subtopics in physics, chemistry, and biology (24). Biophysics is a highly interdisciplinary field that can benefit significantly from skills typically presented in a specialized manner in other disciplines, and TPM is one of such concepts that can be used as a template to demonstrate such interdisciplinary connections. In addition to gaining an understanding of theoretic and experimental principles, students with access to this simulation tool kit in the curriculum can gain exposure to computational, statistical, and mathematic knowledge in the context of a useful topic with "real-world" applications. In its current form, educators can use this TPM tool kit to help students gain an appreciation for basic theory and implementation of theory because all the code is written and commented on in an easily understandable form. Unlike in research contexts in which one is assumed to be able to make these connections without prior education, this TPM simulation GUI assumes only basic mathematic and coding knowledge, with little to no background in the theoretic behaviors of the TPM system itself. Overall, this is a tool kit meant

Table 1. Parameters considered in the TPM simulation. Static refers to fields that are assigned before the TPM simulation starts. Dynamic refers to fields that can be modified during the simulation.

Simulation parameters	Parameter notation
Length of simulation (static)	n
Tether persistence length (static)	L_p
Tether length (static)	L_o
Viscosity of environment (static)	η
Temperature of environment (static)	T
Radius of bead (static)	R_B
Density of bead material (static)	ρ
DNA force (net) (dynamic)	$F = F_x, F_y, F_z$

for students to have a focused interaction in a short activity (e.g., class assignment or project) and that grants access to easily understandable biophysics concepts without the need for complex background knowledge.

III. METHODS

A. Simulation overview

Our simulation experiment considers the dynamics of a bead attached to a surface by using classical physics–based analysis. All the relevant parameters in this model can be altered by the user to explore alternative scenarios that aid in student learning. Further, parameters that are variable in the actual SMFS experimental setups are designed to be dynamic and can be modified by the user in real time during the simulation, mimicking an actual experiment being conducted in real time as well. The static and dynamic parameters associated with a typical single-molecule TPM system are summarized in Table 1.

Based on these parameters, a complete description of the tethered bead position, applied force, intrinsic force due to particle collisions, energy, and tether extension from equilibrium are provided in the form of continually updated graphic plots in a MATLAB-based GUI. These plots are updated at a rate specified by the user in a static field prior to start of the simulation. The interface in which each of these parameters are provided by the user and the key features of the simulation package are summarized in Figure 1.

B. Simulation logic

A single MATLAB function that accepts user-generated parameter space, as well as memory terms, was used. This function is called within a loop in the MATLAB App Designer, and the outputs are plotted at the user specified rate. Callback functions are used in the interface to synchronize the point at which the user makes a change and when that change is reflected in the base code output. The use of memory terms in the app allowed for the computations to be done with continuity, as the user inputs are monitored and updated continuously within the base algorithm. Several simulations of the length specified by the user are run consecutively with initial conditions consistent with the end state of the prior simulation. This results in a continuous generation of data until the user-specified total number of data points are reached. A flow chart of the simulation logic is found in the Supplemental Figure S1. The simulation produces an output file in a comma-separated value (*csv*) format that contains time (s), planar position (*m*), net DNA force (*N*), applied force in *z* (*N*), Cartesian DNA force components (*N*), and θ/φ angular positions (-).

C. Computational framework of the simulation

The notations outlined in Tables 1 and 2 will be used to reference each variable in this work.

The modified Marko–Siggia wormlike chain model was considered for our model in Eq. 1 (25). Numeric root finding was used to solve for the approximate magnitude of the force for each direction.

$$F_i = \left(\frac{k_B T}{4L_p}\left[\frac{1}{(1-\frac{R_i}{L_o}+\frac{F_i}{K_o})^2} - 1 + \frac{4R_i}{L_o} - \frac{4F_i}{K_o}\right]\right), i = x, y, z \quad (1)$$

In this model, the $\frac{F}{K_o}$ terms are a correction introduced to the classic wormlike chain model to account for the elasticity of the tether. This modification improves the experimental

Table 2. Summary of parameter notations used for the MATLAB code and variable descriptions with reference to the defining equation (if applicable). Tether extension (r) and DNA force (net) are the vector quantities of the position and DNA force in x, y and z, respectively.

Parameter of interest	Notation	Equation
Position (Cartesian)	x, y, z	—
Displacement (Cartesian)	$\Delta x, \Delta y, \Delta z$	8, 9, 10
Tether extension (net)	r	—
Spherical angles	θ, φ	6, 7
Potential energy	PE, ΔPE	15
Kinetic energy	KE, ΔKE	16
DNA force (Cartesian)	F_i	1, 3, 4, 5
DNA force (net)	F	—
Time-averaged root-mean-square fluctuation	RMS	21

agreement of the wormlike chain model that provides only an order of magnitude estimate of the persistence and contour lengths (26). The K_o term is a material parameter described by the Young modulus from classical mechanics. In this simulation, the Young modulus was related to the persistence length of a solid rod with a circular cross section for mathematic simplicity (25). The DNA diameter of $d = 1.6$ nm was chosen, and the Young modulus depends on the user-defined temperature and persistence length in Eq. 2. Some typical values of this parameter range from 800 to 1,700 pN (27, 28).

$$K_o = \left(\frac{16k_BT}{d^2}\right)L_p \tag{2}$$

A spherical coordinate system was used to describe the particle's 3-dimensional motion. The obtained magnitude was decomposed into x, y, and z components via projection onto a Cartesian system by using the following elementary trigonometric relations in Eqs. 3–5.

$$F_x = F^*|\sin\theta^*\cos\varphi| \tag{3}$$

$$F_y = F^*|\sin\theta^*\sin\varphi| \tag{4}$$

$$F_z = F^*|\cos\theta| \tag{5}$$

The signs of these quantities were determined directly through the consideration of the extension of the tether. If the tether was extended in a negative direction, the force would have to be positive to restore the system to its equilibrium position and vice versa. This behavior is consistent with classical spring behavior described by Hooke law and serves as a reasonable description for the behavior of the tether–bead system at any point in its motion due to the elasticity of the tether. All these computations were completed in a MATLAB function named *MarkoSiggiaVectorized.m*, and these force computations were continuously updated in a loop from the base code. The Supplemental Material documentation of the simulation package provides greater detail on the functional dependencies.

The computation of the θ and φ positions also come from basic trigonometric relations in Eqs. 6 and 7. The spatial orientation of the system is initially defined to be along the Cartesian z direction alone, and the descriptions of the angles are updated as the motion evolves over time.

$$\theta = \tan^{-1}\left(\frac{\sqrt{x^2+y^2}}{z}\right) \tag{6}$$

$$\varphi = \tan^{-1}\left(\frac{y}{x}\right) \tag{7}$$

Next, the function *TetherForce2.m* base code modifies the implicit force term in the z direction based on the magnitude of external force applied to the system in the user interface. The first option for the user is to choose a modifiable but constant force at any point in the simulation. When the user makes a modification to the applied force using the force slider built into the app, a constant force is continually applied to the system for the duration that the user leaves the slider in the given position. This force is immediately applied with the chosen magnitude. The second option for the user is to apply a force ramp with a slope predetermined by the user. The desired force by the end of the simulation is computed to increase in linear increments consistent with the total run time of the simulation. The third option for the user is to apply a decaying force ramp that is

computationally equivalent to the previous case, except that a linear decay is considered instead. The projection of this magnitude onto the z direction is added to the force term from the MarkoSiggiaVectorized.m function to determine the net force such that $F_{net} = F_z + F_{applied}$, considering the force decomposition based on the second law of Newton.

The net effect experienced by the bead is intended to be consistent with Stokes law. The bead is assumed to be perfectly spherical, surfaces are all assumed to have no imperfections, components are all assumed to be entirely homogenous, and the flow is constrained to be laminar. This means that the system has a low Reynolds number that is consistent with smooth and constant fluid motion (i.e., laminar flow). When the Reynolds number is low, viscous force is necessarily dominant, meaning perturbations introduced by the bead on the system are not the variable that dominates the overall motion. The liquid viscosity is a crucial variable in determining the scale of such effects, and a specific analysis of relevance of the viscosity is presented in Supplemental Figure S3. A numeric validation of these assumptions is provided in the validation section of this study. Because all these conditions are approximately valid in the considered model, Stokes law serves as a reasonable approximation to the net effect that is observed. This also means that enough information is available so that the deviations in position within a given timestep can be extrapolated from the simulation, as is outlined in Eqs. 8–10. A correction factor is introduced to account for the edge effects because the tether–bead system is near the surface throughout the simulation. These corrections are derived based on the boundary condition that tangential flow needs to be zero at the bead surface (29, 30). The x displacement (Δx) is parallel to the surface and is described in Eq. 8.

$$\Delta x \approx \frac{F_x \Delta t}{6\pi\mu R} * \frac{1}{1 - \frac{9}{16}\left(\frac{r}{z}\right) + \frac{1}{8}\left(\frac{r}{z}\right)^3 - \frac{45}{256}\left(\frac{r}{z}\right)^4 - \frac{1}{16}\left(\frac{r}{z}\right)^5} \tag{8}$$

Similarly, the expressions for the y and z directions can also be obtained. The y displacement (Δy) is parallel to the surface, so the correction due to surface effects remains the same.

$$\Delta y \approx \frac{F_y \Delta t}{6\pi\mu R} * \frac{1}{1 - \frac{9}{16}\left(\frac{r}{z}\right) + \frac{1}{8}\left(\frac{r}{z}\right)^3 - \frac{45}{256}\left(\frac{r}{z}\right)^4 - \frac{1}{16}\left(\frac{r}{z}\right)^5} \tag{9}$$

The displacement in z (Δz) is perpendicular to the plane, so the correction due to surface effects is slightly different. This correction results in Eq. 10:

$$\Delta z \approx \frac{F_z \Delta t}{6\pi\mu R} * \frac{1}{\left(1 - \frac{9}{8}\left(\frac{r}{z}\right) + \frac{1}{2}\left(\frac{r}{z}\right)^3 - \frac{57}{100}\left(\frac{r}{z}\right)^4 + \frac{1}{5}\left(\frac{r}{z}\right)^5 + \frac{7}{200}\left(\frac{r}{z}\right)^{11} - \frac{1}{25}\left(\frac{r}{z}\right)^{12}\right)} \tag{10}$$

Here, Eqs. 8–10 are used to update the x, y, and z position at a given timestep. These Cartesian position elements are then used in Eqs. 6 and 7 to update the spatial orientation elements from the initial state due to the viscous motion.

The rearrangement of Stokes law is only an approximation because finite timesteps are used to approximate the velocity of the bead and particle in addition to the numeric approximation of the surface effects. However, an effort was made to more accurately account for time that the particle takes to move between any 2 given positions through the introduction of a dynamic timestep (30) described in Eq. 11.

$$\Delta t = \frac{2\mu\delta R}{|\nabla F|} \tag{11}$$

The implementation of this dynamic timestep allows for the accuracy of the position at any given timepoint to be the same, because the deviation is normalized using the force gradient at every data point (30). The modified Marko–Siggia model accounts for the extensibility of the tether. This has a direct influence on the dynamic timestep that depends on normalization using the force gradient. The explicit computations are shown in Eqs. 12 and 13.

$$\nabla F = \frac{\frac{2}{L_0 d_x} + \frac{4}{L_0}}{\frac{4L_p}{k_B T} + \frac{2}{K_0 d_x} + \frac{4}{K_0}}, \frac{\frac{2}{L_0 d_y} + \frac{4}{L_0}}{\frac{4L_p}{k_B T} + \frac{2}{K_0 d_y} + \frac{4}{K_0}}, \frac{\frac{2}{L_0 d_z} + \frac{4}{L_0}}{\frac{4L_p}{k_B T} + \frac{2}{K_0 d_z} + \frac{4}{K_0}} \tag{12}$$

$$d_i = \left(1 - \frac{i}{L_0} + \frac{F_i}{K_o}\right)^3, \quad i = x, y, z \tag{13}$$

After these predictable effects are accounted for, the last remaining component necessary for accurately describing the particle position is its random motion due to diffusion. The correction factor to the position predicted from the basic force analysis was implemented using a random number generator. The random number generator was set so that the mean value is zero and a standard deviation defined by Eq. 14. The environment is assumed to be approximately isotropic, as previously mentioned, which means that the expected standard deviation is independent of direction.

$$\sigma = \sigma_x = \sigma_y = \sigma_z = \sqrt{2\Delta t \frac{k_B T}{6\pi\mu R_b}} \tag{14}$$

The assumptions outlined previously allowed for a complete description of the position of the bead–tether system to be generated under applied force. Because the time associated with motion between any 2 given positions is also available, many useful computations can be done to test the validity of the code (for example, the verification of the conservation of energy). The general relation $F = -\nabla U$ was considered. The force acting on the particle is approximated to be constant and independent for a given timestep. This means that the potential energy can be approximated using Eq. 15. The force terms are constant in each interval; thus, the integration only occurs over the position differential.

$$\begin{aligned}\Delta PE_i \approx -(&F_x*(x_i - x_{i-1}) + F_y*(y_i - y_{i-1}) \\ &+ F_z*(z_i - z_{i-1}))\end{aligned} \tag{15}$$

The projections of the force on the x, y, and z direction and the displacement as calculated between subsequent timesteps are considered in determining the change in potential energy. The kinetic energy was computed and rewritten using parameters relevant to the constructed system in Eq. 16.

$$\Delta KE_i \approx \frac{2\pi\rho R_b^3}{3} * \frac{(x_i - x_{i-1})^2 + (y_i - y_{i-1})^2 + (z_i - z_{i-1})^2}{(\Delta t)^2} \tag{16}$$

The ρ term in the kinetic energy computation is the density of the bead, the displacement in each direction is determined at subsequent timesteps iterated by variable i, and the length of the timestep is denoted Δt.

All the arguments made previously are consistent with a probabilistic consideration of the behavior of the tether–particle system. This means that by nature, assumptions of thermal equilibrium are made, as can be seen from the applications of the equipartition theorem. These assumptions are not appropriate when a force is instantly applied to the system. The force ramp feature used allows for a steady buildup of the force that does not perturb the system to a great extent at any given instant. However, for general applications of large magnitudes of force, this model can break apart. As such, a separate model was implemented as described in the following, which uses physical constraints to ensure that the system remains stable, as expected in reality.

First, in the cases in which an external force is applied to the system, it is approximated that $F_{net} \approx F_{applied}$. When a force is applied, the tether will extend, and the tension will increase resulting in limited fluctuations. In accordance with the modified Marko–Siggia model (25), these fluctuations will occur with an equilibrium value that is associated with the applied force. Extracting this equilibrium value allows for a description of the bead position to be made independent of the timescale associated with the instability. Generating a distribution of permissible values about this equilibrium position allows for a complete description of the bead position. It is constrained by the tether length, and there is a very small probability the bead will reach a value significantly different from the equilibrium value. These constraints are well described by a normal distribution with 0 mean fluctuations about the equilibrium position. The standard deviation was determined, as

shown in Eq. 17, where α is an arbitrary parameter meant to describe the resistivity of the environment and z_{eq} is the extracted equilibrium position. This parameter is not strictly defined and can be modified to best fit the data collected. In accordance with the assumption of isotropy, $\alpha = 3$ was assigned as the base setting.

$$\sigma_z = \frac{L_o - z_{eq}}{\alpha} \tag{17}$$

Because the z spatial harmonic behavior is described, the planar region of interest can easily be extrapolated. The system is defined so that magnitude of the position vector corresponds to the tether extension. Because a reasonable approximation to the z position is obtained, the acceptable x and y positions must be approximately consistent with the constraint in Eq. 18 because a force regime in which unwinding of the double-stranded DNA occurs ($\sim$65 pN) is not considered here.

$$x + y = L_o - z_{eq} \tag{18}$$

The distribution of the x and y positions are not expected to have significant bias because an isotropic environment is considered. As such, the weight of the permissible positions will be approximated to be equivalent.

Using these 2 conditions, a constraint for the x and y position can be obtained. Because the viscous effects also have a contribution to the planar variations, a distribution was generated under the assumption of thermodynamic equilibrium in Eq. 14. The instantaneous application of force in the z direction is accounted for without the consideration of thermodynamic equilibrium. Essentially, this means that the system is forced into a harmonic state that can be described by conditions using thermodynamic equilibrium. The implementation of the previously described method is a boundary condition that restabilizes the environment. This means that the assumption of thermodynamic equilibrium is valid after the system is constrained with this method. This equilibrium is artificial in the sense that constraining the system requires higher force fluctuation magnitudes than is experimentally observed. A spatial resolution of 10% was used to limit the simulation to values similar to experimental fluctuations; Eqs. 19 and 20 describe the x and y positions of the bead within this framework. The computations done in the simulation begin by considering the origin of the system in the frame of the bead. All the terms were rescaled so that the result is consistent with these relations where x_{visc} and y_{visc} are Brownian terms that account for the viscous motion and possibilities for extension of the tether.

$$y = \frac{(L_o - z_{eq})}{2} + y_{visc} \tag{19}$$

$$x = \frac{(L_o - z_{eq})}{2} + x_{visc} \tag{20}$$

The assumptions made when generating this simulation are consistent with the assumptions made in a typical Markov process (31). The distributions from which the Brownian fluctuations are determined are normal with a mean of 0 and standard deviation defined in Eq. 14. All Brownian fluctuations are extrapolated from probability distributions governed by the same rules, are time independent, and intrinsically constrain how far a particle could be displaced due to a collision with the molecules in the viscous environment. This means that at any given position, the span of reasonable values classically obtainable by the particles is predefined for a given timestep. Finally, each state attained by the particle is assumed to be independent of every subsequent state obtained by the particle. This is consistent with the constraints associated with classical Brownian motion (32).

Within the simulation, there are 2 models implemented. The first, which the simulation is initialized to use as the toggle switch, is the *trend* model. This model is intended only for educational purposes. It is a mixture of both model types mentioned previously, wherein the point at which the first model breaks down

is point in which the new model is implemented. In other words, in absence of force, the probabilistic model, described by Eqs 1–16, and the constraint model, with Eqs 17–20, are both implemented. The first model is purely probabilistic in nature and gives predictions closer to the equilibrium state on average, whereas the second model is much stricter, and the values accepted tend to be more confined. In transitioning between these models, physically unrealistic results may be occasionally observed. However, there are many benefits to this model, as described in the following discussions. For stricter data collection mode, the toggle switch must be switched to *data*, where the numeric inconsistencies from the force application will not exist.

IV. RESULTS

A. Implementation and theoretic validation

All data are generated using 2 primary tiers of code. First, TetherForce2, runs the simulation based on the equations previously described for using loops. Next, a loop in the MATLAB App Designer was used to continually update the arrays containing the parameter space generated. The results generated in the base code based on the updated parameter space are immediately assigned to relevant GUI axes to plot the results, as the simulation continues running in real time. This second tier of code is the most inefficient component of this simulation because it must check for user input at every data point, update the parameters the base function calls at every data point, and plot the data at a rate specified by the user. A more comprehensive discussion of the simulation efficiency is provided in the Supplemental Appendix. In case the code is being used solely for data generation (and not GUI-based results for visualization in real time), the user can set the plot rate equal to the total number of data points, and this will result in significantly improved run time. Although slightly more computationally intensive, it was found that continual application of a force did not significantly affect the run time of the simulation.

Aside from the actual implementation, the simulation gives a reasonable approximation to the physical behaviors associated with a typical tethered particle–bead system. The tether particle–bead system will display a wide range of fluctuations in every direction provided that an external force is not applied to the system. The parameter space used to generate the results plots are outlined in Table 3.

Due to the lack of significant tension on the tether in the absence of an applied force, the planar variation will be more prominent because the tether–bead system will not have any rigidity, as shown in the upper panel of Figure 2.

In the presence of an applied force, it is expected that the particle will asymptotically approach maximum extension over a given time and the *x*–*y* motion will be confined to smaller scales due to the tension exerted by the tether. The lower panel of Figure 2 was generated using the trend mode of the simulation. The details of this mode will be discussed in more detail in the following.

In the absence of an applied force, the planar position of the particle is unrestricted and varies with a span of approximately $\pm$800 nm. In the presence of an applied force, the span in which the planar position varies is limited to approximately $\pm$200 nm. This behavior becomes more evident as the magnitude of the force increases over time because the tether will experience increasing tension. In

Table 3. Sample parameter space used to generate Figure 2 result plots. The parameters are approximately consistent with the simulation parameters considered in the implementation by Beausang et al. (41).

Parameter (unit)	Value
n (–)	10,000
L_o (nm)	1,180
L_p (nm)	72
η (Pa $\times$ s)	0.0089
T (C)	25
R_B (nm)	50
Plot rate	10,000

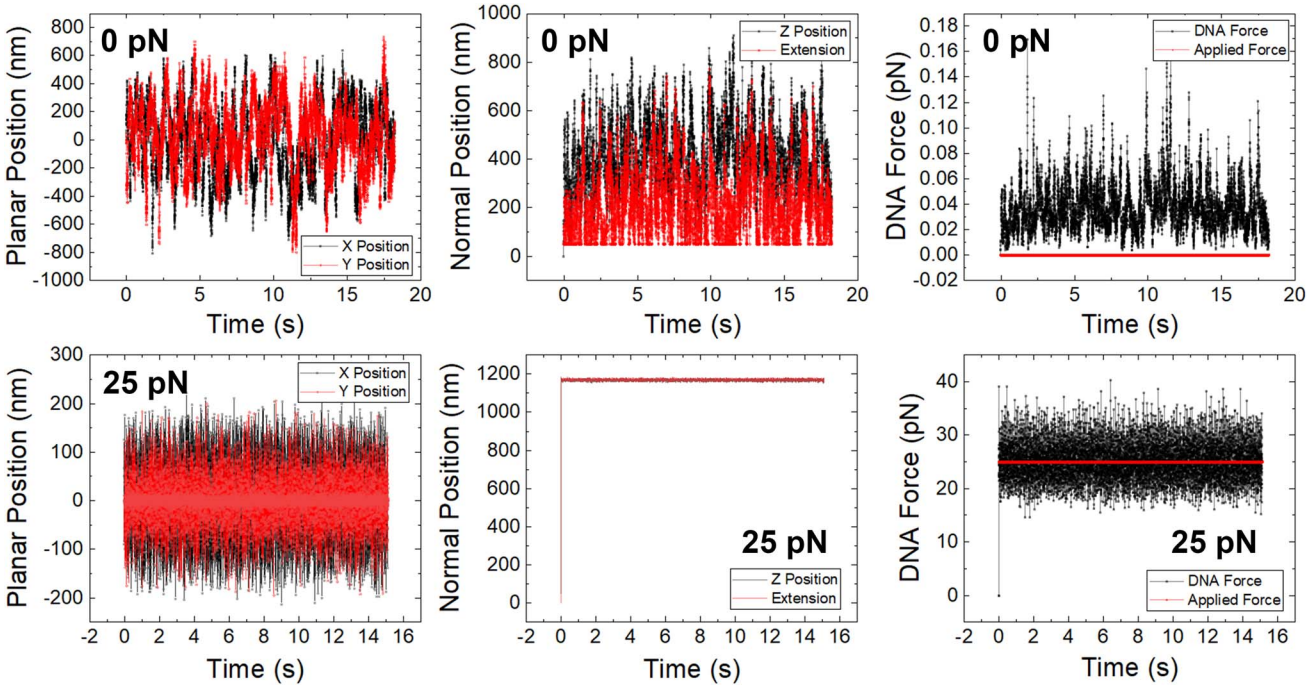

Fig 2. Simulation model predictions for TPM with or without applied force on the system. Upper left panel: planar position (*XY*) versus time in absence of applied force. Upper middle panel: Normal position (*Z*) versus time in absence of applied force. Upper right panel: DNA force versus time in absence of applied force. Lower left panel: planar position (*XY*) versus time in presence of 25-pN applied force. Lower middle panel: normal position (*Z*) versus time in presence of 25-pN applied force. Lower right panel: DNA force versus time in presence of 25-pN applied force. All panels were generated by using the trend mode of the simulation GUI.

presence of an applied force, the system asymptotically fluctuates near maximum extension. All these behaviors are consistent with theoretic expectations.

The final features implemented into this simulation are analysis plots. A useful analysis that validates the results of the simulation is the consideration of the applied and intrinsic DNA forces as a function of the net extension (*r*), presented in Table 2, which represents the magnitude of the 3-dimensional radius vector of the position for each Cartesian component (*x*, *y*, *z*). In this model, the maximum extension should not greatly exceed the combined length of the bead and tether at any time-point because the force application is limited to a regime in which double-stranded DNA helix unwinding is not relevant, as previously discussed. Figure 3 confirms this physical restriction both in the presence and absence of an applied force. Further validation using energy analysis is presented in Supplemental Figure S3.

B. Model validation via AFS experiments

For the comparison of the simulation results with SMFS experimental data, a TPM experiment was carried out in our laboratory by using an Acoustic Force Spectroscopy instrument (AFS) (LUMICKS, Amsterdam, The Netherlands). A more detailed description of the experimental setup is found in the Supplemental Appendix. Briefly, the surface of the AFS chip is incubated with anti-digoxigenin fab fragments for 20 min, followed by surface passivation with bovine serum albumin (BSA) protein, casein protein, and Pluronic F-127 nonionic surfactant in 10 mM phosphate-buffered saline solution for 30 min. Next, DNA functionalized on opposite ends with biotin and digoxigenin is mixed with streptavidin-functionalized polystyrene beads for 30 min, washed twice in PBS containing BSA, casein, and Pluronic F-127, and incubated in the AFS imaging chip for 15 to 30 min. Finally, nonbound beads are flushed out, and the remaining beads are tracked in 3 dimensions. Analysis of bead

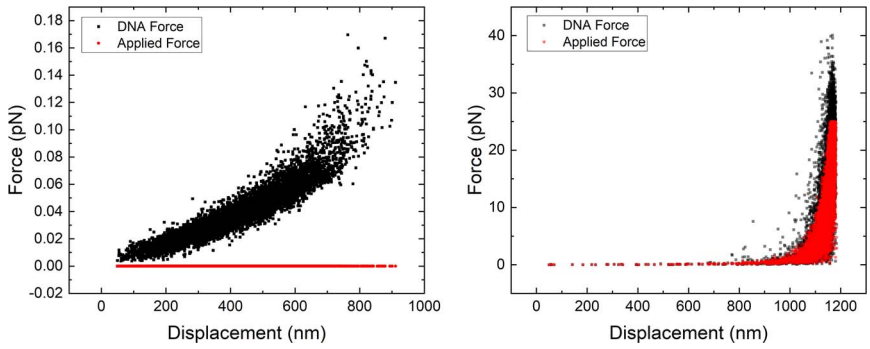

Fig 3. Force extension curves in the absence of force (left) and in the presence of a force ramp up to 25 pN (right). The contour length was set to 1,180 nm, as indicated in Table 3.

traces was performed with the software provided by LUMICKS (AFS-Analysis-G2 version, Amsterdam, The Netherlands), with slight modifications (34), and a free academic version can be found in the original publication of the AFS (22).

As can be observed in Figure 4, the simulated root-mean-square (RMS) position values of the bead–tether systems are of the same order of magnitude and follow the same trend as the AFS experimental values, based on the simulation parameters presented in Table 4. The RMS value (22) was determined by using Eq. 21, where $\overline{x}$ and $\overline{y}$ are the average x and y positions, respectively, of the position coordinates presented in Table 2.

$$\text{RMS} = \sqrt{(x-\overline{x})^2 + (y-\overline{y})^2} \tag{21}$$

As the magnitude of applied force increases, the equilibrium RMS position the system takes decreases. The discrepancy in experimental RMS values is due to experimental limitations such as uncertainty in the exact bead size, resolution of the AFS instrument or technique, and model limitations. Namely, an order of magnitude approximation is being conducted on the basis of previously described assumptions, so while the trends are captured, the model itself does not have a resolution allowing better certainty to be achieved for all types of analysis. In these simulations, the bead diameter was set at 3,110 nm. The bead diameter does not influence the harmonic behavior and affects only the scaling of the time from the earlier described dynamic timestep. The experiments were carried out in phosphate buffer supplemented with low concentrations of proteins and polymers (see Supplemental Material); however, it is assumed that those additives did not change the viscosity (35). Thus, the simulation uses the viscosity of pure water.

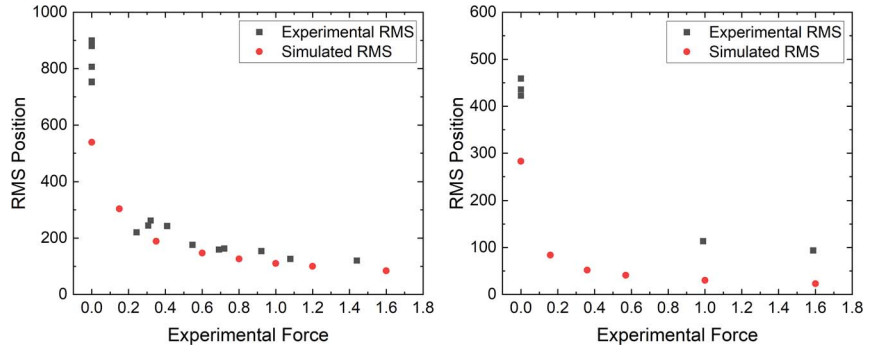

Fig 4. Simulation model trends agree well with TPM observed in AFS experiments. Left: experimental and simulated average *x*/*y* and RMS position values with application of constant force for 1,800-nm DNA strands attached to a polystyrene bead of 3,110-nm diameter in buffer at room temperature. Right panel: experimental and simulated average *XY* and RMS position values with application of constant force for a 500-nm DNA strand attached to a polystyrene bead of 3,110-nm diameter in buffer at room temperature. The larger discrepancy between experimental and simulated RMS for 500-nm tethers is discussed in the text.

Table 4. Sample parameter space used to generate Figure 4 result plots.

Parameter (unit)	Value
n (–)	10,000
L_o (nm)	1,800/500
L_p (nm)	50
η (Pa × s)	0.0089
T (C)	25
R_B (nm)	1,550
Plot rate	10,000

C. Case study demonstrating use of the GUI for TPM modeling in a classroom setting

The following section outlines the question that could be asked by an educator, implementation of the TPM simulation tool kit to address the question, and specific steps taken within the tool kit GUI to obtain a suitable answer generated by the students. One example question posed by the educator to the students could be "How does the time averaged <RMS> value vary as a function of tether contour length in TPM?"

Steps taken by the students or instructor to address this specific question are briefly outlined in the following:

(a) Open the simulation and show the students each of the variable meanings using the definition tab. Emphasize the importance of fixing all variables, except the tether length, because that is the variable of interest.

(b) Assign physically reasonable values (such as the default values) to all the variables, except the tether length, consistent with the type of system that is being studied.

(c) Choice 1: The simulations could be run prior to the lecture, and the output files could be displayed in a suitable dataset format to the instructor's preference.

Choice 2. The class can be divided into groups, and each group can run a simulation for a particular tether length. The results can then be combined for the final plot.

The simulated data are saved in *csv* format in the same folder as the GUI, which contains labeled fields, including the time (s); *x*, *y*, and *z* position data (*m*); the total force (*N*); the applied force (*N*); the *x*, *y*, and *z* components of the force (*N*); and the θ/φ angular positions.

(d) When the simulation is completed, the script *Example_1_script* included with the sample lesson plan can be used to automatically output the RMS values for a given simulation.

(e) The general trends could be displayed through the creation of plots, as shown in Figure 5. Notes about the nature of Brownian motion and the consequent variation in results among trials could be made. To account for such variability, the trials were conducted 3 times per tether lengths, and an average was obtained to generate the figure.

(f) The characteristic behavior in which the RMS value tapers off, as tether length increases (27), should be highlighted by the instructor. Limitations regarding the models in general should be discussed with students.

The raw data used to generate Figure 5 in *csv* format can be found on GitHub (https://github.com/ChundawatLab/TPM-GUI), along with an example to create and analyze force–extension curves, summarized in a lesson plan.

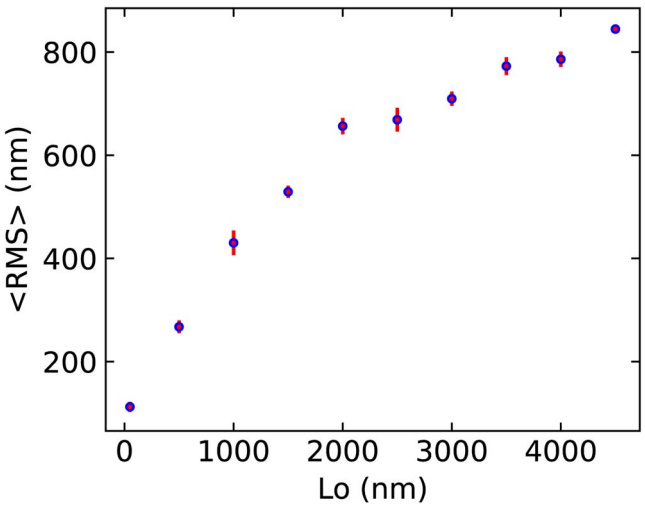

Fig 5. Case study results demonstrating how the TPM GUI can be used by an educator in a classroom setting. Average RMS position calculated from repeating the simulation 3 times per tether length and taking the average of the obtained results. The red vertical bar represents the standard deviation of 3 experimental replicates.

The GitHub material also includes the GUI source code and user guide and manual. Further similar experimental comparisons are included in Supplemental Figures S5–S7. Other points of discussion could be how the behavior of these curves depends on the bead radius, which also tends to be varied in real SMFS experiments. In general, hands-on exploration of the simulation tool kit permits many modes of analysis relevant to actual experiments and provides results that are consistent with the actual trends from real-world experiments so that student learners can gain deeper insight into the concept of TPM.

V. DISCUSSION

In its current setup, our simulation package provides an efficient means of generating an estimate for how a tethered particle–bead system behaves in a viscous fluid environment. The introduction of the extensibility of the tether into the wormlike chain model accounts for the elasticity of DNA when forces are applied (27). However, there are some computational limitations associated with this model. First, a basic reduction reveals that the force model has multiple solutions. As the simulation runs, the numeric solver tends to choose a solution that can best numerically minimize the equation. Although numerically reasonable, the alternate solution is not physically meaningful. Second, all descriptions made in the initial model are developed under the assumption of thermal equilibrium. When a force of sufficient magnitude is applied, the timestep calculation that depends inversely on the force gradient becomes infinitesimally small. This results in the computations of the position terms becoming unreasonable as well because position terms depend on the timestep. Consequently, a new model was implemented to preserve the validity of the assumptions of thermodynamic stability throughout the simulation. Specifically, 2 models were implemented into our simulation interface: trend analysis and data collection only, as was mentioned in section III.C.

The trend model captures the overall behaviors exhibited by the system. There are some numeric inconsistencies that exist in the model. In transitioning between a state of stability and artificial stability, the planar position will display a slight increase in magnitude of fluctuations. This is consistent with expectation, because the constraints inherently require the system to achieve a length consistent with the tether length. The values attainable by the particle strictly in the probabilistic approach of the trend model tend to be closer to the equilibrium state, but the span is not so strictly constrained. These methods represent different forms of numeric approximations, and these discrepancies become evident as the simulation runs. The physical constraints provide an upper limit to the acceptable planar position values attained by the system, whereas the probabilistic approach represents the average expected fluctuations. This is optimal for use in a classroom setting, as learners can be exposed to the differences in different approximation techniques, while simultaneously understanding that models are not exact. Rather, every model has a limitation, and one needs to understand the differences in the nature of models to find the best one for one's needs. For the purposes of strict data collection, the data mode is designed only to use the physically constrained model, eliminating the transition point and providing data that can be used for comparisons with previous studies, as shown in Supplemental Figures S5–S7 and discussed in the Supplemental Material document.

A more precise model would require consideration of the bending of DNA beyond the persistence length considered in the wormlike chain model. The bending of the molecular structure of DNA on smaller scales than the persistence length is an experimentally known fact, and the wormlike chain model does not account for this (36). Theoretically, this phenomenon can be accounted for through consideration of the elastic collisions between the molecular bond sites and photons that result in small-scale bending, a phenomenon characterized as Raman scattering

that can be modeled with molecular dynamics and quantum mechanics and molecular mechanics modeling techniques (37). However, such algorithms are computationally intensive. The semiflexible polymer description of the modified wormlike chain model that considers a single persistence length serves as a good approximation of the average of the individual base-pair contributions and is sufficient for a general user trying to understand TPM.

For general cases, we have shown there is reasonable agreement between the predictions of the TPM simulation model and AFS experimental results. Studies have been conducted that attribute specific protein functionality to the manner in which it biases the Brownian motion that the proteins are undergoing (38). Although such effects are experimentally observable, there is no general way of accounting for the binding dynamics of all protein and tether combinations. This simulation is written in a manner in which specific systems can easily be considered. For instance, the construction of the bead and tether are done through experimentally modifiable quantities, such as material density and stress tolerance. This means an extension can easily be made to transform the algorithm, perhaps through the implementation of a bead subfunction, into a simulation more representative of any given protein–ligand system of interest. As previously mentioned, the MarkoSiggiaVectorized.m subfunction also provides a way for the user to easily modify the expected DNA force fluctuations by implementing corrections that more adequately account for specific systems of study. Overall, this simulation is a template that can be easily generalized to be made relevant to any specific area of teaching.

In an educational context, the simulation is designed to promote student learning. The code is written so that the student can follow through the logic and go through the derivations done to solve for all the outputs from first principles. All the assumptions made are outlined in the comments of the MATLAB code. Although we have not tested our simulation in an actual classroom setting, several studies have been conducted to determine the effects of using computational sciences and simulations in a classroom setting to promote student science, technology, engineering, and math learning. Allowing students to work through simulations alone rather than offering step-by-step guidance is often observed to result in better learning outcomes, although there are indications that the amount of prior knowledge a learner has may have an effect on what they are able to extract from online content (39, 40). In some similar studies, the use of simulations was found to promote knowledge integration processes, which implies that students were able to form a deeper level of understanding of the material due to exposure to the material (41). The results for these types of studies tend to be diverse due to the extensive number of confounding variables present in such trials. However, these studies tend to compare the effectiveness of simulation-based versus classical instruction–based learning, and it is widely found that both provide similar results for evaluating pedagogic effectiveness. This simulation package with an easy-to-follow GUI was created with the intention of providing students and instructors the opportunity to quickly review a highly relevant topic in modern physics and engineering in a very short amount of time that would otherwise not be covered in a typical undergraduate curriculum.

The simulation is quick to set up and produce results; hence, a few minutes are long enough to extrapolate all the noticeable trends associated with a tether–particle system. The simulations could be used within a typical 60–80 min instructional lecture period. Further, the students could be tasked with using the code to do more detailed analysis such as model fitting for the data because the code outputs all relevant data. Questions could also be asked about the logic used to develop the model, because the manipulations made are clearly defined. Elementary knowledge of physics and trigonometry is all that is necessary to follow the logic for early undergraduate

students, even if they cannot understand the finer details. Upper-level undergraduate students should be able to follow the logic and derive every relation considered by using the given models. Force–extension curves and RMS position analysis for data analysis are highly valuable tools for students to gain an understanding of tethered particle systems.

VI. CONCLUSIONS

This work describes a simulation for TPM that comes with a customizable user interface. By using the modified wormlike chain model with suitable corrections due to geometric constraints, a simulation capable of predicting trends consistent with experimentally obtained data of TPM was demonstrated. By using the MATLAB App Designer, a user interface was created that allows users to interactively modify parameters in the simulation, as they would be able to do if they were conducting an actual SMFS or TPM experiment. Trials were set up to validate our simulation through consideration of behaviors in limits, verification of assumptions made, and comparison to actual experimental data, as well as demonstrating a use case for teaching purposes. All these tests indicated that the simulation provides a reasonable classical description of TPM.

Some fundamental limitations of the simulation are associated with the instability in the probabilistic approach and the consideration of a fixed persistence length. Even so, having a sense of the dynamics of DNA scale or similar polymer–tether systems will allow students to gain an intuitive understanding and insight into what can be expected from single-molecule experiments using advanced techniques such as optical tweezers or AFS. As advanced imaging tools gain more traction both in the real world (e.g., point-of-care diagnostics) and academic world (e.g., single-molecule imaging of cellular biophysical phenomena), it becomes imperative to expose students (and future scientists) early on to such techniques in a classroom setting with an appropriate simulation tool kit.

SUPPLEMENTAL MATERIAL

All supplemental material is available at: https://doi.org/10.35459/tbp.2022.000238.

AUTHOR CONTRIBUTIONS

KR, MH, and SPSC designed the research, MH and KR conducted the research, and KR, MH, and SPSC wrote the manuscript.

ACKNOWLEDGMENTS

SPSC acknowledges support from the Rutgers University Aresty Research Center and the National Science Foundation (Chemical, Bioengineering, Environmental and Transport Systems award 1846797). KR acknowledges Rujuta Mokal for reviewing logic and providing support in the development of the code and writing of the article. MH thanks Tan Ngo for help in the initial stages of this study. The authors declare no competing interests.

REFERENCES

1. Brinkers, S., H. R. C. Dietrich, F. H. De Groote, I. T. Young, and B. Rieger. 2009. The persistence length of double stranded DNA determined using dark field tethered particle motion. *J Chem Phys* 130:215105. http://doi.org/10.1063/1.3142699.
2. Heller, I., T. P. Hoekstra, G. A. King, E. J. G. Peterman, and G. J. L. Wuite. 2014. Optical tweezers analysis of DNA-protein complexes. *Chem Rev* 114:3087–3119.
3. Jungmann, R., M. Scheible, and F. C. Simmel. 2012. Nanoscale imaging in DNA nanotechnology. *Wiley Interdiscip Rev Nanomed Nanobiotechnol* 4:66–81.
4. Schafer, D. A., J. Gelles, M. P. Sheetz, and R. Landick. 1991. Transcription by single molecules of RNA polymerase observed by light microscopy. *Nature* 352:444–448.
5. Gelles, H. Y. L. R. J. 1994. Tethered particle motion method for studying transcript elongation by a single RNA polymerase molecule. *Biophys J* 67:2468–2478.
6. Igarashi, K., T. Uchihashi, T. Uchiyama, H. Sugimoto, M. Wada, K. Suzuki, S. Sakuda, T. Ando, T. Watanabe, and M. Samejima. 2014. Two-way traffic of glycoside hydrolase family 18 processive chitinases on crystalline chitin. *Nat Commun* 5:1–7.
7. Igarashi, K., T. Uchihashi, A. Koivula, M. Wada, S. Kimura, T. Okamoto, M. Penttila, T. Ando, and M. Samejima. 2011. Traffic jams reduce hydrolytic efficiency of cellulase on cellulose surface. *Science* 333:1279–1282. https://doi.org/10.1126/science.1208386.
8. Brady, S. K., S. Sreelatha, Y. Feng, S. P. S. Chundawat, and M. J. Lang. 2015. Cellobiohydrolase 1 from *Trichoderma reesei* degrades cellulose in single cellobiose steps. *Nat Commun* 6:10149.
9. Hilton, M. A., H. W. Manning, I. Górniak, S. K. Brady, M. M. Johnson, J. Zimmer, and M. J. Lang. 2022. Single-molecule investigations of single-chain cellulose biosynthesis. *Proc Natl Acad Sci U S A* 119: e2122770119. http://doi.org/10.1073/pnas.2122770119.
10. Bustamante, C. J., Y. R. Chemla, S. Liu, and M. D. Wang. 2021. Optical tweezers in single-molecule biophysics. *Nat Rev Methods Prim* 1:25. https://doi.org/10.1038/s43586-021-00021-6.
11. Abbondanzieri, E. A., W. J. Greenleaf, J. W. Shaevitz, R. Landick, and S. M. Block. 2005. Direct observation of base-pair stepping by RNA polymerase. *Nature* 438:460–465.
12. Comstock, M. J., K. D. Whitley, H. Jia, J. Sokoloski, T. M. Lohman, T. Ha, and Y. R. Chemla. 2015. Direct observation of structure-function relationship in a nucleic acid–processing enzyme. *Science* 348:352–354.

13. Svoboda, K., C. F. Schmidt, B. J. Schnapp, and B. S. M. Block. 1993. Direct observation of kinesin stepping by OT interferometry. *Nature* 365:721–727.
14. Finer, J. T., R. M. Simmons, and J. A. Spudich. 1994. Single myosin molecule mechanics: piconewton forces and nanometre steps. *Nature* 368:113–119.
15. Chundawat, S. P. S., B. Nemmaru, M. Hackl, S. K. Brady, M. A. Hilton, M. M. Johnson, S. Chang, M. J. Lang, H. Huh, S.-H. Lee, J. M. Yarbrough, C. A. López, and S. Gnanakaran. 2021. Molecular origins of reduced activity and binding commitment of processive cellulases and associated carbohydrate-binding proteins to cellulose III. *J Biol Chem* 296:100431. http://doi.org/10.1016/j.jbc.2021.100431.
16. Newton, M. D., B. J. Taylor, R. P. C. Driessen, L. Roos, N. Cvetesic, S. Allyjaun, B. Lenhard, M. E. Cuomo, and D. S. Rueda. 2019. DNA stretching induces Cas9 off-target activity. *Nat Struct Mol Biol* 26:185–192.
17. Deng, Y., and W. Lv. 2016. Biofilms and Implantable Medical Devices: Infection and Control. In Woodhead Publishing Series in Biomaterials. Elsevier Science, Amsterdam, The Netherlands.
18. Chandrasekhar, S. 1949. Brownian motion, dynamical friction and stellar dynamics. *Dialectica* 3:114–126.
19. Kumar, S., C. Manzo, C. Zurla, S. Ucuncuoglu, L. Finzi, and D. Dunlap. 2014. Enhanced tethered-particle motion analysis reveals viscous effects. *Biophys J* 106:399–409.
20. Sitters, G., N. Laurens, E. J. De Rijk, H. Kress, E. J. G. Peterman, and G. J. L. Wuite. 2016. Optical pushing: a tool for parallelized biomolecule manipulation. *Biophys J* 110:44–50.
21. Sitters, G., D. Kamsma, G. Thalhammer, M. Ritsch-Marte, E. J. G. Peterman, and G. J. L. Wuite. 2014. Acoustic force spectroscopy. *Nat Methods* 12:47–50.
22. Kamsma, D., R. Creyghton, G. Sitters, G. J. L. Wuite, and E. J. G. Peterman. 2016. Tuning the music: acoustic force spectroscopy (AFS) 2.0. *Methods* 105:26–33.
23. Deniz, A., S. Mukhopadhyay, and E. Lemke. 2008. Single-molecule biophysics: at the interface of biology, physics and chemistry. *J R Soc Interface* 5:15–45.
24. Wang, M. D., H. Yin, R. Landick, J. Gelles, and S. M. Block. 1997. Stretching DNA with optical tweezers. *Biophys J* 72:1335–1346.
25. Epstein, C., and A. Mann. 2012. Measurement of the DNA spring constant using optical tweezers. *Nat Commun* 14:1–2.
26. Smith, S. B., Y. Cui, C. Bustamante, and S. B. Smith. 1996. Overstretching B-DNA: the elastic response of individual double-stranded and single-stranded DNA molecules. *Science* 271:795–799.
27. Broekmans, O. D., G. A. King, G. J. Stephens, and G. J. L. Wuite. 2016. DNA twist stability changes with magnesium(2+) concentration. *Phys Rev Lett* 116:1–5.
28. Happel, J., and H. Brenner. 1983. Low Reynolds Number Hydrodynamics. 3rd edition. Matinus Nihjoff Publishers, The Hague, the Netherlands.
29. Visser, E. W. A. 2017. Biosensing based on tethered particle motion. PhD thesis, Eindhoven University of Technology: the Netherlands.
30. Van Kampen, N. G. 2007. Markov processes. In Stochastic Processes in Physics and Chemistry, third edition. N. G. Van Kampen, editor. Elsevier, Amsterdam, pp. 73–95. https://www.sciencedirect.com/science/article/pii/B9780444529657500076.
31. Chandrasekhar, S. 1943. Stochastic problems in physics and astronomy. *Rev Mod Phys* 15:1–87.
32. Hackl, M., E. V. Contrada, J. E. Ash, A. Kulkarni, J. Yoon, H.-Y. Cho, K.-B. Lee, J. M. Yarbrough, C. A. López, S. Gnanakaran, and S. P. S. Chundawat. 2022. Acoustic force spectroscopy reveals subtle differences in cellulose unbinding behavior of carbohydrate-binding modules. *Proc Natl Acad. Sci U S A* 119:e2117467119.
33. Galush, W. J., L. N. Le, and J. M. R. Moore. 2012. Viscosity behavior of high-concentration protein mixtures. *J Pharm Sci* 101:1012–1020.
34. Ramdin, K. A., M. Hackl, and S. Chundawat. 2023. TPM-GUI. (Version 1.0.0) [Computer software]. https://github.com/ChundawatLab/TPM-GUI.
35. Wiggins, P., T. Van Der Heijden, F. Moreno-Herrero, A. Spakowitz, R. Phillips, J. Widom, C. Dekker, and P. C. Nelson. 2006. High flexibility of DNA on short length scales probed by atomic force microscopy. *Nat Nanotechnol* 1:137–141.
36. Rao, S., S. Raj, B. Cossins, M. Marro, V. Guallar, and D. Petrov. 2013. Direct observation of single DNA structural alterations at low forces with surface-enhanced Raman scattering. *Biophys J* 104:156–162.
37. Ishii, Y., Y. Taniguchi, M. Iwaki, and T. Yanagida. 2008. Thermal fluctuations biased for directional motion in molecular motors. *BioSystems* 93:34–38.
38. Chang, K. E., Y. L. Chen, H. Y. Lin, and Y. T. Sung. 2008. Effects of learning support in simulation-based physics learning. *Comput Educ* 51:1486–1498.
39. Al Mamun, M. A., G. Lawrie, and T. Wright. 2022. Exploration of learner-content interactions and learning approaches: the role of guided inquiry in the self-directed online environments. *Comput Educ* 178:104398. http://doi.org/10.1016/j.compedu.2021.104398.
40. Taub, R., M. Armoni, E. Bagno, and M. Ben-Ari. 2015. The effect of computer science on physics learning in a computational science environment. *Comput Educ* 87:10–23.
41. Beausang, J. F., C. Zurla, L. Finzi, L. Sullivan, and P. C. Nelson. 2007. Elementary simulation of tethered Brownian motion. *Am J Phys* 75:520–523.